ADVANCED MATERIALS TECHNOLOGIES
www.advmattechnol.de

Quantification of the Deep Discharge Induced Asymmetric Copper Deposition in Lithium-Ion Cells by Operando Synchrotron X-Ray Tomography

Shahabeddin Dayani, Henning Markötter,* Jonas Krug von Nidda, Anita Schmidt, and Giovanni Bruno*

Lithium-ion cells connected in series are prone to an electrical safety risk called overdischarge. This paper presents a comprehensive investigation of the overdischarge phenomenon in lithium-ion cells using operando nondestructive imaging. The study focuses on understanding the behavior of copper dissolution and deposition during overdischarge, which can lead to irreversible capacity loss and internal short-circuits. By utilizing synchrotron X-ray computed tomography (SXCT), the concentration of dissolved and deposited copper per surface area is quantified as a function of depth of discharge, confirming previous findings. The results also highlight for the first time a nonuniform distribution pattern for copper deposition on the cathode. This research provides insights for safer battery cell design.

1. Introduction

Lithium-ion batteries are one of the most popular energy storage solutions for electric vehicles, mainly thanks to their high gravimetrical energy density. Battery cells are usually connected in series and parallel to meet required voltage and current demand of such vehicles. However, the load profile of an electric vehicle is very unpredictable, comprehending high current demands during charge and discharge caused by acceleration and regenerative braking, respectively.[1] Thus, the ageing of individual cells is hard to predict and can result in cells with different states of health within one battery. If connected in series, such cells are more prone to an electrical abuse, called overdischarge.[2]

Overdischarge occurs when a cell is discharged beyond its predetermined lower voltage limit, dictated by the cell chemistry. Overdischarge has been shown to cause gas formation, mainly carbon dioxide, carbon monoxide and methane accompanied with heat generation in the cell.[3] Many studies have reported copper dissolution from the current collector when the cell is overdischarged.[3–5] This has been reported to be the cause of irreversible capacity loss and internal short circuits in cells.[2,4] Recharging the damaged cells could cause potential thermal runaway hazards, as a result of short-circuits induced by dissolved copper.[2]

In this paper the terms *overdischarge* and *deep discharge* are used to describe different scenarios during battery discharge. Overdischarge is referred to when the discharge process is halted upon reaching 0 V, while deep discharge refers to the situation where the discharge continues after the cell voltage is negative.

Generally, the initial step during an overdischarge involves the further deintercalation of lithium ions from the anode, and their intercalation into the cathode. This causes an increase in the anodic potential and a decrease in the cathodic potential, thus, leading to the observed fast drop in cell voltage. However, due to the typically lost lithium in the first cycle(s) caused by Solid Electrolyte Interphase (SEI) formation, the cathodic potential initially drops rather slowly whereas the anodic potential rises quickly. If the anode potential surpasses the oxidation potential of copper, i.e., E^0 (Cu/Cu^{2+}) = 0.34 V versus standard hydrogen electrode (SHE) and 3.38 V versus Li/Li^+, the copper foil can start to oxidize. Utilizing this value in a simplified manner for a LIB-cell and assuming a cathode potential of approximately 3.7 V versus Li/Li^+, copper oxidation could start at a cell voltage of approximately 0.3 V. If the overdischarge process is stopped at this stage, recharging the cell causes the majority of the oxidized copper ions to deposit again as metal on the anode side. However, if overdischarge is followed by deep discharge, leading to a negative cell voltage, the dissolved copper ions within the electrolyte migrate through the separator and can be reduced into metallic copper on the cathode.[2]

The mechanism of an overdischarge down to a cell voltage of 0 V has been investigated in several studies. An irreversible capacity loss was reported for overdischarging LiCoOx / graphite cells.[4] Moreover, the formation of gases at this stage of discharge has also been reported. Such gas formation can be correlated to the decomposition of the solid electrolyte interphase (SEI) due to excess de-intercalation of lithium ions from the anode

S. Dayani, H. Markötter, J. K. von Nidda, A. Schmidt, G. Bruno
Bundesanstalt für Materialforschung und -Prüfung (BAM)
Unter den Eichen 87, 12205 Berlin, Germany
E-mail: shahabeddin.dayani@bam.de; henning.markoetter@bam.de

The ORCID identification number(s) for the author(s) of this article can be found under https://doi.org/10.1002/admt.202301246

DOI: 10.1002/admt.202301246

leading to the aforementioned increase in anodic potential.[3] The before discussed possibility to oxidize the copper current collector as a result of overdischarge was also shown in multiple publications[2–4] Using X-ray photoelectron spectroscopy and X-ray absorption fine structure (XAFS), Cu-dissolution has been confirmed to be even detectable at a rather high cell voltage of 0.5 V in a cell with lithium nickel cobalt aluminum oxide (NCA) as cathode active material.[6]

Due to the inability of the typically implemented Battery Management System (BMS) to monitor individual cell voltages in a large battery pack, lithium-ion cells connected in series could undergo voltages beyond 0 V while the battery pack is being discharged. Therefore, it is of importance to study the overdischarge mechanism also *below* 0 V. If overdischarge is not stopped, the anode potential keeps raising and cathode's potential keeps decreasing. As mentioned, if the anode potential reaches the copper oxidation potential, Cu is oxidized to Cu^{2+} ions. Consequently, oxidized Cu^{2+} ions can migrate through the anode matrix and potentially traverse the separator, ultimately reaching the cathode. If the deep discharge condition persists, these ions can be reduced and deposited as metallic copper onto the cathode surface.[7] Guo et al. found that after breakdown of the SEI at 110% depth of discharge (DoD), oxidation of Cu started at around 112% DoD. Several studies have reported that if the cell is discharged between 110–120% DoD, its recharge is not possible due to severity of the internal short circuits (ISC).[2,8,9] EDX observations confirmed that the Cu concentration on the cathode is several times higher than on the anode if deep discharge continues beyond 150% DoD.[7,10]

In,[3] it was found that in a lithium cobalt oxide/graphite cell the oxidation of elemental copper to copper ions takes place when the potential of the anode rises to 3.4 V versus Li/Li+. which corresponds to a cell voltage of 0.2 V. Li et al. have prevented an anode potential increase by adding 20 weight percent of Li(NiCoMn)Ox to Lithium Cobalt Oxide. This addition resulted in much less dissolved copper in comparison to the original anode chemical composition. To increase the resilience of lithium-ion cells against overdischarge, lithium titanium oxide has been reported to be a candidate for anode material. Using this anode material, deep discharged cells (up to 140% DoD) could be recharged.[8]

To better understand the overdischarge and deep discharge mechanisms, in situ and ex situ imaging techniques have been used. In a study by Harding et al., cross section SEM imaging of the aged cells was employed to show that while using NCA as cathode active material, a lithium titanate oxide (LTO) anode is more resistant to overdischarge than graphite. SEM/EDX showed that copper is dissolved and dispersed in the graphite anode matrix whereas a cell with LTO anode shows nearly no dissolution of the aluminum anode current collector. Cu deposition on the NCA cathode was also not observed in the graphite based cells.[11]

Due to its nondestructive nature, X-ray computed tomography (XCT) is a powerful tool to study mechanisms of ovrdischarge and deep discharge. Bond et al. have studied a lithium cobalt oxide / graphite cell under deep discharge down to −0.5 V using synchrotron-based XCT (SXCT) and could confirm swelling of the cell due to gas formations.[12] The effect of deep discharge on a 18 650 type cell with NCM cathode material was studied using lab based XCT by T. Ma et al.[13] The cell was discharged using a 1C current up to 150% DoD; however, no visible Cu dissolution was observed using XCT images whereas SEM images of the disassembled cell could image Cu deposition on both cathode and anode. In another study, Cu pits on the anode current collector was observed by ex-situ XCT of an electrode piece of a 18 650 cell with LiFePo4 cathode, which was suffered overdischarge during a high cycle operation.[5]

Generally, the literature results confirm the mentioned mechanism during a deep discharge as well as overdischarge of a LIB-cell. However, the results also show nicely, that the exact onset of Cu-oxidation as well as amount and place of Cu-plating highly depends on, e.g., the anode/cathode material used, the capacity balancing of the two electrodes and the electrochemical procedure applied.

In the present study, we employ SXCT as a nondestructive method to quantify deep discharge phenomenon on a commercial lithium-ion cell. The mechanism of this electrical abuse is identified. We also quantify the mass of copper per surface area dissolved from the current collector and deposited onto the cathodes as a function of depth of discharge (DoD). This allows a comprehensive understanding of the discharge process, thus, enabling tailor-made designs to prevent such an electric abuse.

2. Experimental

2.1. Sample Information

A 7×7×4 mm^3 commercial pouch cell with $LiCoO_2$ (LCO) as cathode active material with a nominal capacity of 30 mAh was used for deep discharge experiments. The size of this pouch cell is optimal for electrode level SXCT investigations.[14]

2.2. Electrochemical Tests

Battery cycling experiments were conducted using a Gamry 1010 potentiostat. The pouch cell was fully charged using constant-current (CC) charging rate of 1C, current was set to 1 times the battery's nominal capacity, to 4.2 V and was kept at that voltage (CV) until the current rate fell below 0.1C. The cell was then discharged at constant-current (CC) rate of C/3 until it reached a cut-off voltage of 1 V. After a short open circuit voltage step, discharge with the same current continued without any cut-off voltage limit.

2.3. Synchrotron X-ray Computed Tomography

SXCT experiments were done at the imaging station BAM*line*,[14,15] which is located in the BESSY II synchrotron facility operated by the Helmholtz–Zentrum Berlin (HZB). Projections were acquired using a parallel monochromatic X-ray beam with an energy of 48 keV at an effective pixel size of 0.72 µm. The rotating table at the BAM*line* imaging set up is equipped with a slip ring, which eases the connection of the cell with the potentiostat during SXCT

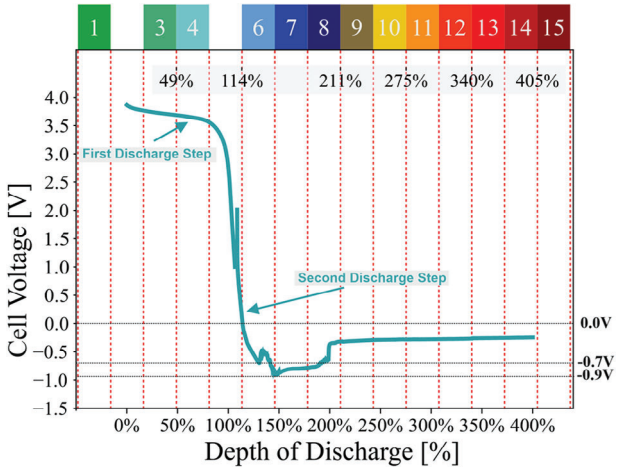

Figure 1. Deep discharge voltage profile versus depth of discharge. Colored boxes indicate duration of each SXCT measured at that depth of charge.

measurements. Each SXCT measurement consists of 3000 projections over a total 180-degree rotation and takes 25 minutes to complete. The battery was being operated during imaging experiments.

Reconstructions were performed using a home-made software based on the Tomopy package[16] optimized for batch reconstruction of SXCT images- 4D reconstruction. Image analysis was performed using self-written python scripts using common data analysis libraries. The 3D rendered images were generated by the software Dragonfly.[17]

3. Results and Discussion

Figure 1 shows the voltage versus depth of discharge curve during two constant current discharge steps interrupted by a short open circuit voltage step. The depth of discharge is defined as percentage of discharged capacity per maximum available capacity of the cell. The discharge curve resembles a deep discharge behavior reported by multiple references.[2,9] After the lithium deintercalation phase, there is a rapid decrease in cell voltage at around 114% DoD reaching a local minimum at −0.7 V followed by another dip to −0.9 V at 150% DoD. The voltage curve reaches a plateau at 200% DoD. Such a plateau is believed to correlate with continuous copper dissolution on the anode and Cu^0-deposition on the cathode, as known from typical electrochemical stripping/plating experiments of metals.[7]

The duration of each SXCT experiment is visualized on the voltage graph. Due to blur caused by movements within the battery's jelly roll during the measurement, the second and fifth SXCT scans were not suitable for further analysis. Colored numbers on top of Figure 1 represent the number of consecutive SXCT scans measured during the deep discharge experiment. All SXCT volumes (volume 3 to 15) were registered to the first volume (volume 1).

In **Figure 2**a complete overview of a cross section of the cell is shown. Three subsets (labelled 1–3) are enlarged to show details. For quantitative analysis, several sub volumes were cropped from region 4. These sub volumes are shown in Figure S1 (Supporting Information).

The degree of copper oxidation varies across different regions within the jelly roll, indicating that the severity of copper dissolution is not uniform throughout the cell. In the middle of the cell, the copper current collector exhibits nearly complete dissolution, while it is less dissolved in the edge areas. This might be due to the nonuniform heat generation in the middle of the jelly roll during the deep discharge experiment, making the center of the cell a more active region compared to other parts of the cell.[18]

The aluminum current collector is coated on both sides with lithium cobalt oxide cathode material, to distinguish between the inner and outer sides, they are shaded in blue and red colors, respectively. The higher X-ray attenuation of copper compared to the cathode allows visually tracking its presence on the cathode material (the brighter spots on the cathode marked by yellow arrows on enlarged regions in Figure 2). There are some regions where copper is deposited on both sides of the cathode, mostly in the middle of the cell, such as in the magnified region number 3 (Figure 2) however it seems the deposition of copper is predominantly occurring on the outer side cathode, highlighted in red. In most regions, the copper deposition appears to have a mossy-like structure. This could be due to the relatively low discharge current chosen for the experiment. However, there are instances, such as in region 3, where a dendritic-like deposition of copper can also be observed, suggesting localized conditions contributing to its formation.

Figure 3 illustrates the progression of the deep discharge experiment by horizontally arranging stripes of a selected volume from region B at several stages of the discharge (Figure S1, Supporting Information). This visualization provides an insight into the Cu deposition as the depth of discharge increases. In Figure 3, the colors and numbers associated with each stripe correspond to those in Figure 1. The horizontal bright layer located in the middle of the montaged stripes, represents the copper current collector that is covered on both sides by the graphite anode and separated from cathodes on either side by a thin separator. In region B, the upper visible cathode, ≈ 210 to 280 µm on the y axis, corresponds to the inner cathode (highlighted in blue), while the lower cathode, approximately 0 to 55 µm on the y axis, corresponds to the outer cathode (highlighted in red). No visible copper dissolution is observed until reaching approximately 81% depth-of-discharge, corresponding to SXCT number 4. Copper dissolution becomes noticeable after reaching a depth-of-discharge (DoD) of 146%, accordingly, in the 6th SXCT. However, the deposition is not yet clearly visible at this stage. Subsequently, the dissolution of copper and its deposition on the outer cathode continues from the 7th SXCT till the end of the experiment.

The line profile of attenuation coefficient is shown for all selected volumes during the deep discharge experiment in Figure 3. Cathodes and copper current collector regions are marked on the graph. As the depth-of-discharge (DoD) increases, the attenuation of the copper current collector, which corresponds to the average density of copper within the current collector, decreases. While DoD increases, a peak form at approximately 50–70 µm on the y-axis. This peak indicates accumulation of copper on the surface of the cathode material. This can lead to closure of ion transportation pathways and, therefore, to permanent damage in

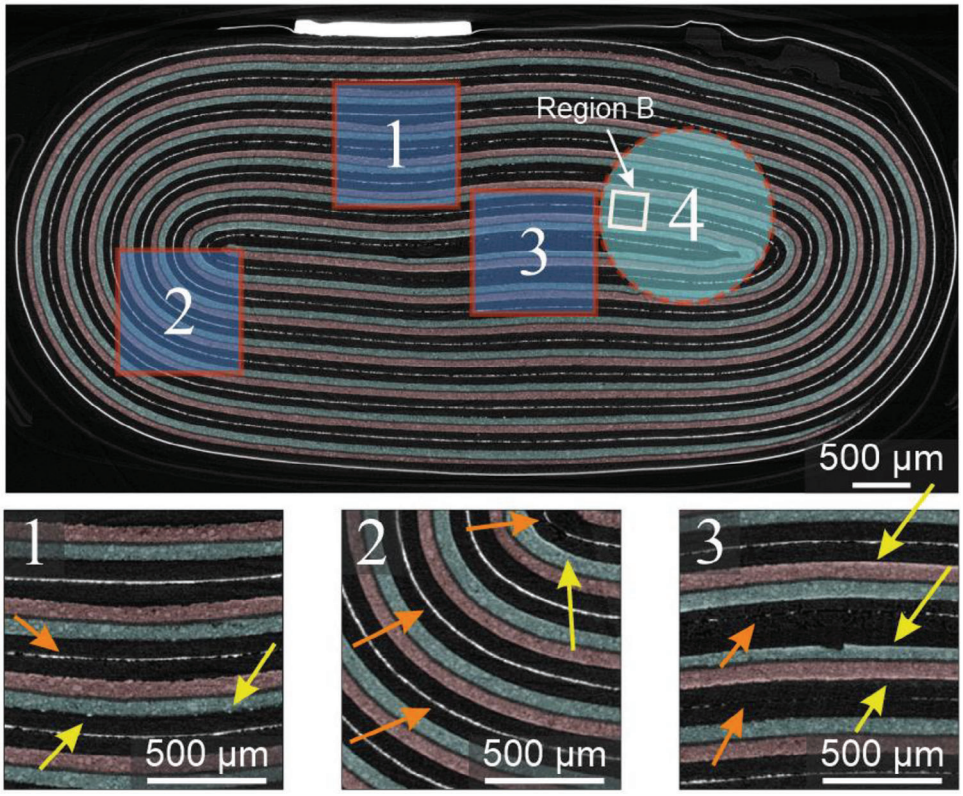

Figure 2. Synchrotron X-ray Computed Tomography (SXCT) of the deep discharged cell at the final stage. Top, overview of jelly roll and copper current collector. Bottom, magnified view of regions 1–3 marked in top figure. Orange arrows point to the copper current collector and yellow arrows show the deposition of copper on the cathode. Inner and outer cathode sides are highlighted with blue and red colors, respectively. Region of interest tomography (ROI) was continuesly performed on the region 4 marked with circle. (for colors, please refer to the electronic version).

these regions. The copper deposition exhibits an asymmetric behavior, favoring the outer cathode.

The same quantities plotted in Figure 3 are plotted in Figure S2 (Supporting Information) for regions A, C and D. The copper deposition in regions A and D shows similar behavior to region B, where the outer cathode is favored for copper deposition. Only in region C, the inner cathode is favored for copper deposition, primarily due to the inaccessibility of the outer cathode for the innermost copper current collector.

The initial (Vi) and final (Vf) states of the deep discharge experiment in region B are depicted in **Figure 4**. Mathematical subtraction of Vi from Vf results into the right-hand side map in Figure 4. Copper removed from and deposited onto the current collector are shown in red and blue, respectively. Asymmetrical deposition of the copper is clearly visualized in this image. This

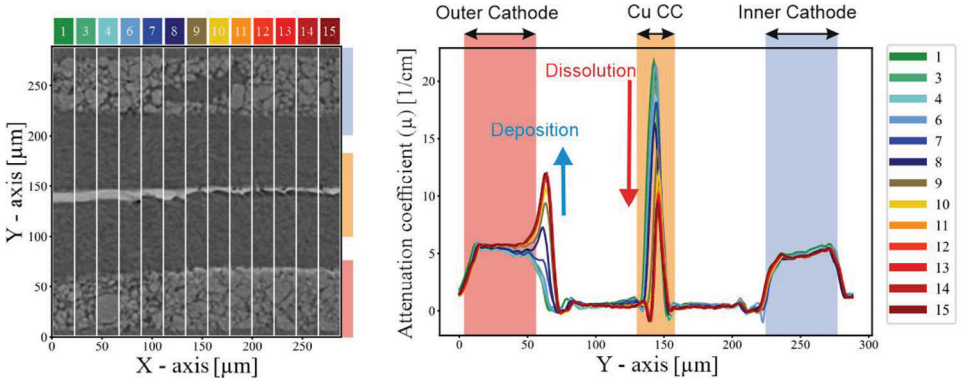

Figure 3. Left, time arrangement of SXCTs from region B from the Figure S2 (Supporting Information) during the deep discharge experiment. Right, plotted attenuation coefficient profile of x-z planes against y position of region B during the deep discharge experiment. (for colors, please refer to the electronic version).

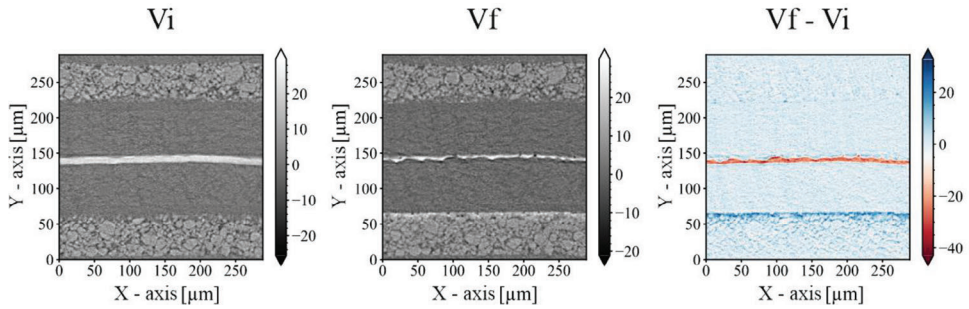

Figure 4. SXCT slice of region B. left, Vi is the initial state of the selected volume, middle, Vf is the final state, right, Vf-Vi is the difference of the final and initial state. (for colors, please refer to the electronic version).

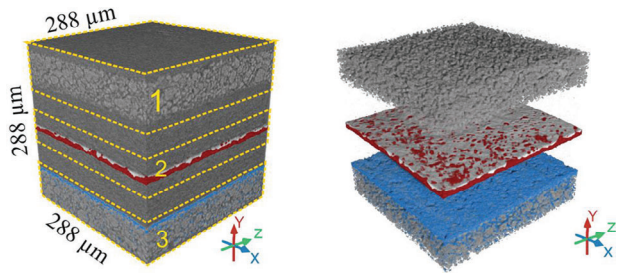

Figure 5. 3D volume rendering for region B in the final stage of the deep discharge experiment. Removed Cu (in control volume 2) is marked in red and deposited Cu on either cathode side is marked in blue. This cubic volume is 288^3 μm^3. (for colors, please refer to the electronic version).

representation is used also in Figure S1 (Supporting Information) to visualize asymmetrical deposition of the copper in various spots of the cell.

3.1. Quantitative Analysis

Due to the high contrast of copper compared to the anode material, segmentation of the current collector (region 2 in **Figure 5**) was performed using thresholding segmentation for all 13 DoD states. The mass of copper m_{Cu} in the current collector was calculated via the number of segmented Cu voxels (n_{Voxels}) using the following equation:

$$m_{Cu} = n_{Voxels} \times V_{voxel} \times \rho_{Cu} \quad (1)$$

where ρ_{Cu} is the density of copper and V_{voxel} is the volume of one voxel. The first selected state is referred to as the *reference state*; with no copper dissolution and no deposition. The amount of copper removed from the current collector is calculated based on the difference between the mass of copper present in each state and the reference state at the selected DoD. To quantify the amount of deposited copper on cathode electrodes of each side (regions 1 and 3 in Figure 5), we employed a different approach. First, the difference of attenuation for each volume was calculated with subtracting that volume from the *reference volume*. It was assumed that the most significant measured differences observed could be attributed to the deposition of copper, as visualized in Figure 4. A control volume was selected as shown in Figure 5 for each cathode region (regions 1 and 3). The attenuation coefficients of all DoD states were subtracted from the *reference state*, thereby yielding the attenuation coefficient of the deposited copper on each cathode side, highlighted with blue color in Figure 5. The average of the difference in attenuation is then calculated along y direction for each x-z plane. Integrating this average function along the y axis equals to the change in attenuation in the control volume. Therefore, the deposited mass of copper per cathode surface area (averaged within the control volume) could be calculated as:

$$m_{Cu}/A = \frac{\rho_{Cu}}{\mu_{Cu\ at\ 48keV}} \times \int \mu(y)\, dy \quad (2)$$

where $\epsilon_{Cu\ at\ 48keV}$ is 26/cm and A is the cathode's geometric surface area.

The described calculations for both deposited and removed copper during the deep discharge experiment was performed on regions A to D (in Figure S1, Supporting Information). To account for statistical deviations, each region was divided into 10 equal sub-regions in the z direction.

Results of the calculations for region B are shown in **Figure 6**. Copper dissolution (oxidation) and deposition (reduction) reactions start above 150% depth-of-discharge and continue with a high and constant reaction rate to about 200% DoD. The reaction rate decreases in the final stage of the experiment. Beyond 350% DoD, it is observed that the copper area density increases to a smaller degree. Even though the total deposited copper and

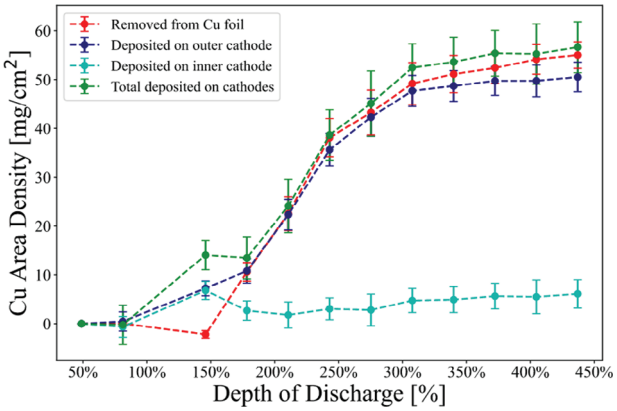

Figure 6. Removed and deposited copper mass per cathode area for region B during the deep discharge experiment plotted against the depth of discharge. (for colors, please refer to the electronic version).

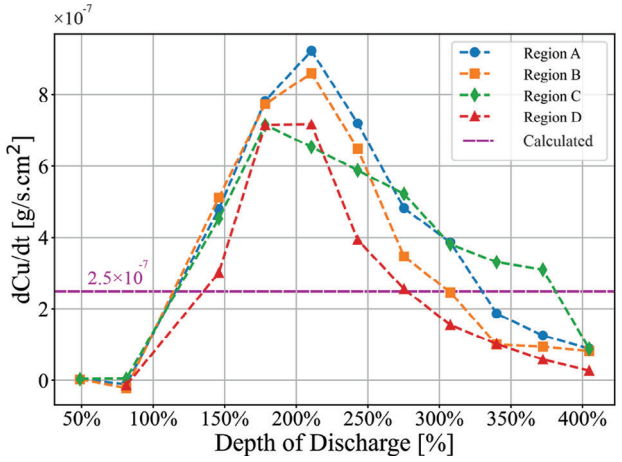

Figure 7. First derivative of amount of removed copper per unit area in respect to time for regions A to D.

the total removed copper from the current collector are calculated using two different methods, their values are within the statistical deviation of each other, except at DoD of 150%. The origin of this discrepancy is a slight motion blur in 6th SXCT. This artifact made it impossible to match it to the *reference volume* (see Figure S3, Supporting Information).

Calculations for other regions shown in Figure S3 (Supporting Information), confirm the similarity of the observed behavior across all quantified regions. Notably, Langner et al. have reported a similar curve for the concentration of copper within the electrolyte of an NMC 622 / graphite cell during a deep discharge experiment, measured using a high-resolution continuum source atomic absorption spectrometer.[19] Despite the difference in measurement methods, the results align consistently with our findings, further validating the reliability and coherence of the observed behavior.

The theoretical average copper oxidation reaction rate is $2.5 \times 10^{-7} g\, s^{-1}\, cm^{-2}$ This value is calculated for a total oxidation of Cu to Cu^{2+} based on the following equation:

$$r = \frac{I \times M}{A \times F \times n} \tag{3}$$

Where, I is the total cell current (10 mA), M is the molar mass of copper (63.5 gr mol^{-1}), F is the Faraday constant ($96.485 \times 10^{+3}$ s.A / mole), A is the total geometrical active electrode surface (13 cm^2) and n is number of electrons transferred per oxidation reaction (2). It is assumed that after 100% DoD total current drawn from the cell is consumed for the striping/plating reaction. The calculated theoretical reaction rate provides a rough estimation based on the calculated active cathode area of the entire cell. However, when comparing this estimation with the quantified reaction rates obtained through image analysis, as depicted in **Figure 7**, it becomes evident that the theoretical estimation is remarkably close.

The reaction rate curve reaches its maximum around 200% DoD for all regions and subsequently begins to decline towards zero as the DoD approaches 400%. Regions A, B, and D exhibit similar reaction rates throughout the deep discharge process. However, in region C, the reaction rate deviates from the other regions after 150% DoD. Between 150% and 280% DoD, the reaction rate in region C is lower compared to regions A and B. Interestingly, in contrast to the other regions, the reaction rate in region C decreases slower, ranging from 4 to 3 $\times$ 10^{-7} g s^{-1} cm^{-2}, between 300% and 375% DoD.

As discussed, the quantification of the stripped and plated copper during deep discharge reveals a clear trend in the oxidation rate of copper during the discharge process. Initially, during the early stages of deep discharge, the rate of copper oxidation is notably high. However, as the process progresses, the oxidation rate begins to decline. This decrease is attributed to ion transport limitations caused by the voids on cupper current collector. Eventually, as these limitations become more prominent, the copper oxidation rate approaches zero in quantified regions. It must be noted that the regions used for the calculations (A-D) represent only a small fragment of the volume mostly in the center of the cell. Since the overall potential of the cell is constant after 200% DoD, the oxidation and reduction reaction are still occurring however not in the field of view of our analysis. Other regions are expected to show a similar behavior. At present, it is not possible to observe the whole cell volume with the desired tomographic resolution to conduct a precise comparison.

4. Summary and Conclusion

The over discharge phenomenon in a commercial cobalt oxide / graphite lithium-ion cell was quantified using operando nondestructive synchrotron X-Ray imaging. This approach allowed us to noninvasively observe the behavior of a cell under such abusive conditions during operation. The results of this study validate and align with previous findings regarding the dissolution of copper and its subsequent migration through the separator, as well as the deposition of copper on the cathode surface when the discharge voltage is allowed to drop beyond the safety limits. The main findings of this study could be summarized as below:

- The degree of copper oxidation varies across different regions within the jelly roll, indicating that the severity of copper dissolution is not uniform throughout the cell. Oxidation of the copper current collector is more severe in the middle of the cell suggesting nonuniform overpotential across the cell which might be due to a nonuniform heat generation in the center of the cell.
- Our observations reveal an unsymmetrical nature of copper deposition during deep discharge. We observe a strong preference for copper deposition on the outer cathode in most regions, although there are specific cases, where the inner cathode is favored due to limited accessibility of the outer cathode.
- The copper oxidation mass per unit area for several regions is calculated and the trend is found to be generally similar across all calculated regions. Some minor differences in the reaction rate and the amount of copper mass oxidized is observed, however the overall trend remains consistent.
- The copper oxidation mass per unit area plotted against DoD exhibits a similar trend to that observed by T. Langner et al. for copper concentration in electrolyte during deep discharge which was measured by a different methodology. This finding provides strong evidence for the validation of our approach

against conventional methods and underlines the advantage of the nondestructive 3D imaging technique.
- Interestingly, the calculated theoretical reaction rate closely resembles the quantified average reaction rate obtained from our analysis.

Using the presented method, further studies can deepen our comprehension of the overdischarge phenomenon to understand the effect of various cathode active materials, discharge current densities and cell designs on the degree and rate of the cell damage. The results of such studies could lead to optimization of the battery design or implementation of protective measures to prevent or mitigate the effects associated with copper deposition, such as capacity loss, increased resistance.

Supporting Information

Supporting Information is available from the Wiley Online Library or from the author.

Acknowledgements

The authors would like to express their gratitude to Michael Sintschuk and Ralf Britzke for the support provided at the Imaging station of the BAM*line*. They also extend their thanks to Martinus Putra Widjaja for the valuable assistance in image segmentation.

Open access funding enabled and organized by Projekt DEAL.

Conflict of Interest

The authors declare no conflict of interest.

Data Availability Statement

The data that support the findings of this study are available from the corresponding author upon reasonable request.

Keywords

battery safety, deep discharge, lithium-ion battery, operando X-ray Computed Tomography, overdischarge, synchrotron X-ray computed tomography

Received: August 3, 2023
Revised: November 6, 2023
Published online:

[1] P. Keil, A. Jossen, *J. Electrochem. Soc.* **2017**, *164*, A3081.
[2] R. Guo, et al., *Sci Rep* **2016**, *6*, 30248.
[3] H.-F. Li, J.-K. Gao, S.-L. Zhang, *Chin. J. Chem.* **2008**, *26*, 1585.
[4] H. Maleki, J. N. Howard, *J. Power Sources* **2006**, *160*, 1395.
[5] R. Carter, B. Huhman, C. T. Love, I. V. Zenyuk, *J. Power Sources* **2018**, *381*, 46.
[6] C. E. Hendricks, A. N. Mansour, D. A. Fuentevilla, G. H. Waller, J. K. Ko, M. G. Pecht, *J. Electrochem. Soc.* **2020**, *167*, 090501.
[7] C. Fear, D. Juarez-Robles, J. A. Jeevarajan, P. P. Mukherjee, *J. Electrochem. Soc.* **2018**, *165*, A1639.
[8] C. Menale, S. Constà, V. Sglavo, L. Della Seta, R. Bubbico, *Energies* **2022**, *15*, 8440.
[9] X. Lai, Y. Zheng, L. Zhou, W. Gao, *Electrochim. Acta* **2018**, *278*, 245.
[10] D. Juarez-Robles, A. A. Vyas, C. Fear, J. A. Jeevarajan, P. P. Mukherjee, *J. Electrochem. Soc.* **2020**, *167*, 090558.
[11] J. R. Harding, B. Han, S. B. Madden, Q. C. Horn, *Energies* **2022**, *15*, 1405.
[12] T. Bond, J. Zhou, J. Cutler, *J. Electrochem. Soc.* **2016**, *164*, A6158.
[13] T. Ma, S. Wu, F. Wang, J. Lacap, C. Lin, S. Liu, M. Wei, W. Hao, Y. Wang, J. W. Park, *ACS Appl. Mater. Interfaces* **2020**, *12*, 56086.
[14] S. Dayani, H. Markötter, A. Schmidt, M. P. Widjaja, G. Bruno, *J. Energy Storage* **2023**, *66*, 107453.
[15] H. Markötter, M. Sintschuk, R. Britzke, S. Dayani, G. Bruno, *J Synchrotron Radiat* **2022**, *29*, 1292.
[16] D. A. Gürsoy, F. De Carlo, X. Xiao, C. Jacobsen, *J Synchrotron Radiat* **2014**, *21*, 1188.
[17] Dragonfly 2020.2 [Computer software]. http://www.theobjects.com/dragonfly (accessed: 2022).
[18] M. Guo, R. E. White, *J. Power Sources* **2014**, *250*, 220.
[19] T. Langner, T. Sieber, J. Acker, *Sci Rep* **2021**, *11*, 6316.